3D Kinetic Monte Carlo Simulation of Electromigration in Multi-layer Interconnects

Linlin Cai, Wangyong Chen, Xing Zhang, Yudi Zhao+, and Xiaoyan Liu*
Institute of Microelectronics
Peking University
Beijing 100871, China
Email: +zhaoyd@pku.edu.cn; *xyliu@ime.pku.edu.cn;

***Abstract*—A 3D kinetic Monte Carlo simulator is developed to describe the electromigration (EM) behaviors in multi-layer interconnects based on the proposed physical mechanism including the metal ions activation, hopping and aggregation processes. The effects of e-wind, hydrostatic stress and Joule heat on EM are implemented in the simulator. The void locations in two directions of upstream and downstream current flow are well reproduced by the simulator, consistent with the experimental observations. The microscopic void morphology and EM degradation are investigated with different operation schemes.**

Keywords—kinetic Monte Carlo simulator, electromigration, interconnect, void

I. Introduction

The electromigration (EM) reliability of back-end-of-line (BEOL) becomes more challenging in high-density integration due to the contradiction between the scaled cross-sectional area and excessive current density [1-3]. The EM simulation by atomic kinetic Monte Carlo (KMC) method provides a better physical understanding of vacancies motion and void formation, also gives the guidelines of interconnects design and reliability prediction [4-5].

In this work, a 3D KMC simulator is developed to capture the void evolution and EM degradation in multi-layer interconnects. The microscopic physical mechanism coupled with the impacts of electron wind (e-wind), stress and heat is proposed and applied to the simulator. The void locations and EM failure with different current operations are investigated by using the simulation tool.

II. Simulation Method and Validation

The microscopic mechanism of EM contains the physical processes of metal ions activation, hopping and aggregation, as shown in Fig. 1. The hopping direction is dominated by the e-wind which can be hindered by the stress- and electric field-induced backflow. The interface barrier $E_{h,i}$ is lower than the bulk barrier $E_{h,b}$ according to the material characteristic [6]. Due to the fact that the metal ions migration trends to the minimum energy locations, the ions with the least nearest ion numbers (n_{ij}) have the smallest activation energy E_a. The metal ions with more n_{ij} are easier to aggregate, which contributes to the void formation. The probability equations of ions motion are described as (1-3) by considering the coupling effects of e-wind, stress and temperature in (4-10) [7-8].

$$P_a = f \cdot \exp\left(-(E_a(n_{ij}) - \Delta E)/k_B T\right) \quad (1)$$

$$P_h = f \cdot \exp\left(-(E_h - \gamma E_{ew} - \lambda E_{st})/k_B T\right) \quad (2)$$

$$P_{ag} = f \cdot \exp\left(-(E_{ag}(n_{ij}) - \Delta E)/k_B T\right) \quad (3)$$

$$E_{ew} = -Z^* eU \quad (4)$$

$$I = U / R_1 \quad (5)$$

$$I = \sinh(\alpha U)/R_2 \quad (6)$$

$$E_{st} = -\Omega \cdot \Delta\sigma_i \quad (7)$$

$$\Delta\varepsilon_i = -f_i \Omega \quad (8)$$

$$\varepsilon_{i,k} = -\nu\sigma_{i,klm}\delta_{ik}/E + (1+\nu)\cdot\left(\sigma_{i,klm}\delta_{il} + \sigma_{i,klm}\delta_{im}\right)/2E \quad (9)$$

$$C \cdot \partial T/\partial t = \nabla(k \cdot \nabla T) + Q \quad (10)$$

Where ΔE is the electric field modulated barrier. I is the node current in the resistor network, U is the potential difference between two adjacent nodes. γ, λ, α are the fitting coefficients. $\Delta\sigma_i$ is the hydrostatic stress gradient, and $\Delta\varepsilon_i$ is the lattice strain deformation. T is the local temperature and Q is the Joule heat power density. The simulated parameters and related physical quantities are listed in Table I.

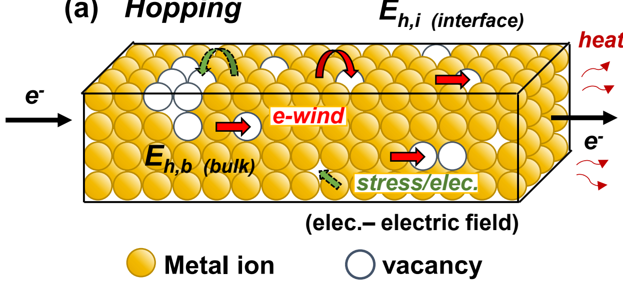

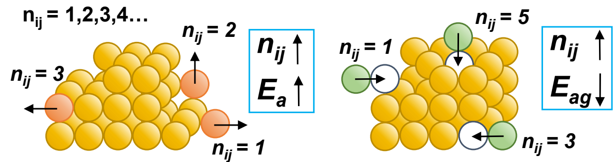

Fig. 1. Microscopic physical behaviors of metal ions during the EM degradation: (a) hopping (b) activation (c) aggregation.

Fig. 2 shows the EM simulation flowchart. The initial parameter input depends on the simulated metal material and size. The grain boundaries are randomly generated by KMC method. The electrical properties of interconnects are calculated by the developed 3D-resistor network with cross nodes [9]. The lattice strain is introduced by vacancy relaxation factor f_i, which stands for the deformation between vacancy volume and atom volume. The relations of lattice strain and stress conform to Hooke's law. The Joule heat is calculated by Fourier equation of heat conduction. Each metal ion motion is determined by comparing the probabilities of different events. Once the ions distribution is changed, the

978-1-7281-0940-4/19/$31.00 ©2019 IEEE

node potential, current, stress gradient and local temperature would be updated. The simulator visualizes the void microscopic evolution and investigates the resistance-time degradation during EM as well as the prediction of time to failure (TTF).

TABLE I. SIMULATION PARAMETERS IN THIS WORK

Symbol	Value	Description
$E_{h,i}$	0.9 eV	Hopping barrier at interfaces
$E_{h,b}$	1.1 eV	Hopping barrier in bulk
$E_{a,nij=1}$	0.85 eV	Activation energy
$E_{ag,nij=1}$	0.8 eV	Aggregation energy
f	10^{13} Hz	Vibration frequency
R_1	$10^2\,\Omega$	Resistance between two ions
R_2	$10^6\,\Omega$	Resistance between ion and vacancy or two vacancies
Z^*	4	Effective charge
Ω	1.6×10^{-23} cm^3	Atom volume
f_i	0.9	Vacancy relaxation factor
E	130 GPa	Young's modulus
v	0.34	Poisson's ratio
C	3×10^6 J/K·m^3	Thermal capacity
k	380 W/K·m	Thermal conductivity

Interconnects	Width	Height
M1-M2	10 nm	20 nm
Via	8 nm	24 nm

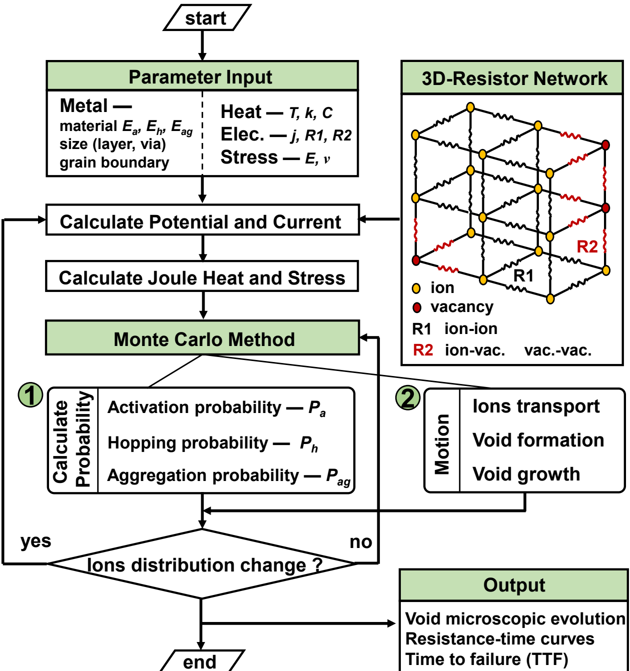

Fig. 2. The EM simulation flowchart. The potential and current distribution are calculated by 3D resistor network.

The simulator is further validated with the experimental measurements [10]. Fig. 3-4 indicate that the simulated results show the excellent agreements with the measured resistance-time curves and cumulative failure distribution respectively. The hopping barrier affected by e-wind and stress plays the dominant role in controlling the TTF of EM. The changes of relative resistance before and after the EM failure are determined together by R_1 and R_2. The gradual increase of resistance after the failure is due to the void lateral growth along the metal wires. The statistic failure distribution is simulated by considering the differences of grain boundaries and the variations of metal ions movements. The resistivity of copper is calibrated with the different metal line widths for the following EM evaluation at 7nm technology node, as shown in Fig. 5 [11].

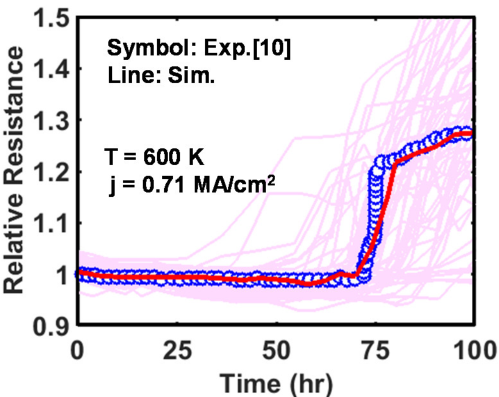

Fig. 3. The simulated resistance-time curves compared with experiment [10] during the EM degradation.

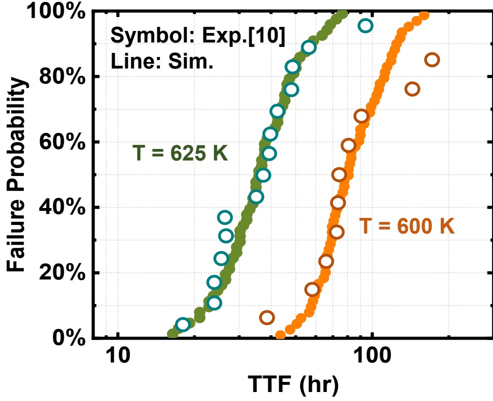

Fig. 4. Cumulative failure distribution between simulation and experiment [10] at different temperatures.

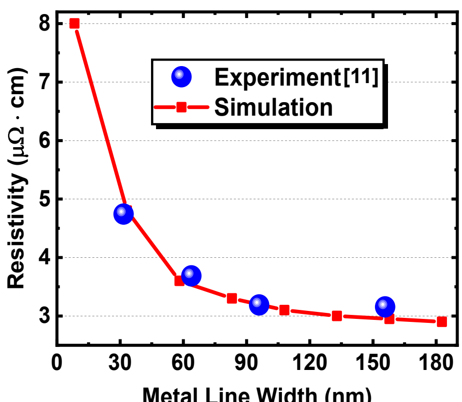

Fig. 5. Calibration of simulated copper resistivity at scaled nodes with experiment [11].

III. RESULTS AND DISCUSSION

Fig. 6 (a) shows the void formation in M1-via-M2 Cu interconnects with upstream current flow. It can be seen that the interconnects are fragile at the via regions near M1 as well

as the corner of via to M2 due to the shift of metal ions driven by the upstream current flow, which is consistent with the experimental FIB-SEM image in [10]. The concentrated vacancies in the via increase the local current density of the wire, leading to the large Joule heat as shown in Fig. 6 (b)-(c). The increased temperature accelerates the void growth, further aggravates the EM degradation. The void evolution over time including the void accumulation, full void formation and growth is shown in Fig. 6 (d). The EM of interconnects undergoes failure after the full void formation in the via. And the void size becomes shrinking over time only when the current flow is cut off. From Fig. 6 (e), the slight recovery of resistance can be found at 600K without the power input of interconnects. Here the EM failure is defined as the 20% resistance increase of initial state.

Fig. 7 shows the simulated EM degradation with downstream current flow from M2 to M1. From Fig. 7 (a), the

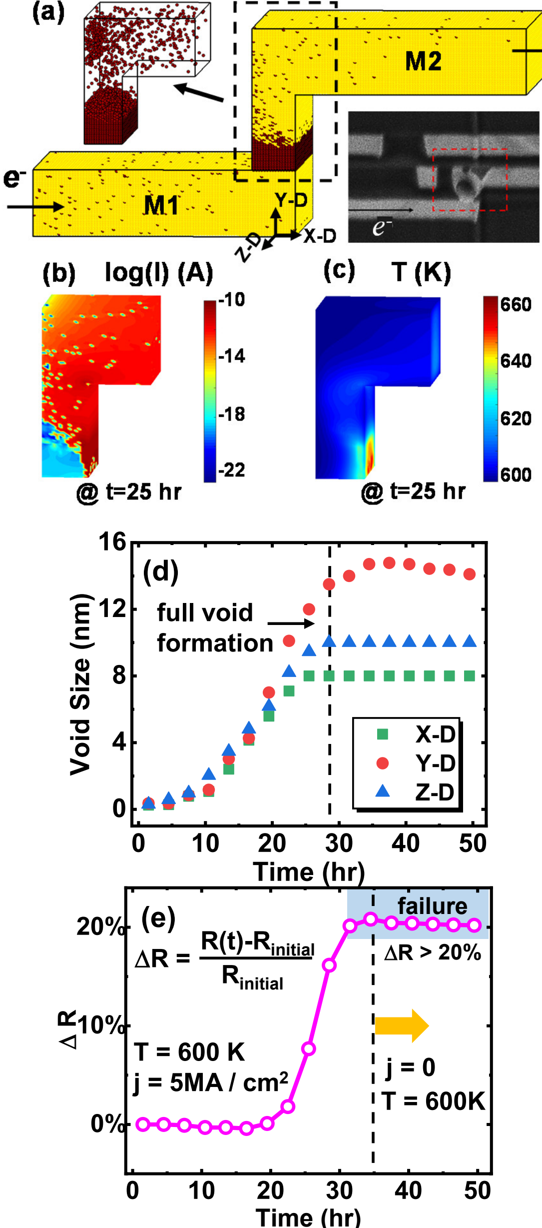

Fig. 6. Upstream current flow from M1 to M2 in EM simulation. (a) void formation in the via compared with FIB-SEM image [10] (b)-(c) local current and temperature distribution of via-M2 (d) void accumulation, full void formation and growth over time (e) R-t curve.

void location is visualized at the M1 regions under the via corresponding to the experimental observation in [12]. The related current and temperature distribution at 25 hours are demonstrated in Fig. 7 (b)-(c). The results show that the void formation with the downstream current flow is slower than that with the upstream current flow, as shown in Fig. 7 (d). And the resistance in Fig. 7 (e) indicates the less degradation and more recovery compared to Fig. 6 (e) due to the incomplete void formation.

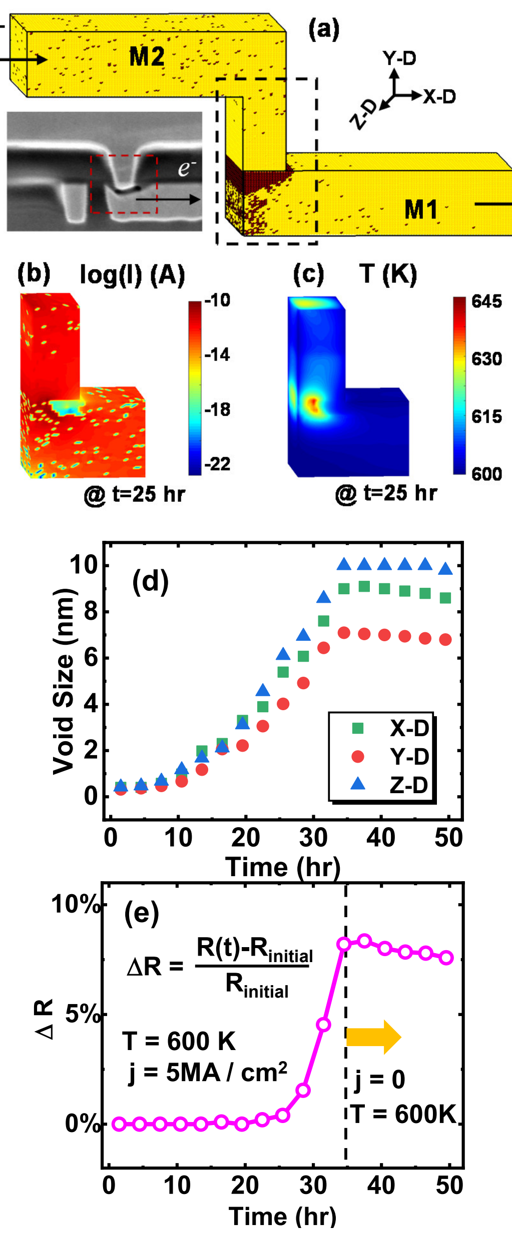

Fig. 7. Downstream current flow from M2 to M1 in EM simulation. (a) void formation in M1 under the via compared with experimental observation [12] (b)-(c) local current and temperature distribution of via-M1 (d) void size evolution over time (e) R-t curve.

Three cases of different current operations of interconnects are investigated in Table II. The results in Fig. 8 present that the void forms at the middle of interconnects in Case I with the unidirectional current. Adding the current branch from the left via, M2 shows the better EM in Case II in comparison with Case I because the metal ions migration driven by the left current fills up the vacancies in the middle of line. However, the interconnects with the bidirectional current operation in

Case III suffer the worst resistance degradation due to the superposed influence of vacancies. The void locations and EM degradation in three cases at 600K are summarized in Table II.

TABLE II. THREE CASES OF CURRENT OPERATIONS OF INTERCONNECTS

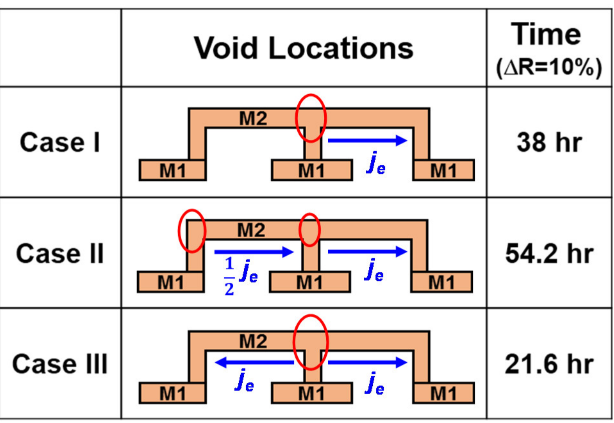

	Void Locations	Time (ΔR=10%)
Case I	M2, M1, M1, M1, j_e	38 hr
Case II	M2, M1, M1, M1, $\frac{1}{2}j_e$, j_e	54.2 hr
Case III	M2, M1, M1, M1, j_e, j_e	21.6 hr

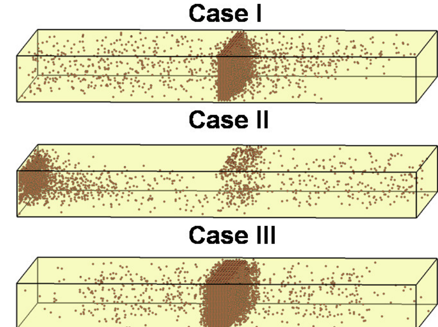

Fig. 8. The void morphology in M2 during EM degradation in three cases of current operations.

IV. CONCLUSIONS

The 3D KMC simulator including the physical behaviors of metal ions is developed to investigate the EM reliability with the coupling effects of e-wind, stress and Joule heat. The simulator validated by the experimental results can well visualize the void locations in interconnects with both upstream and downstream current flow. The void morphology and resistance degradation during the EM simulation are successfully captured with different current operations in three cases. The simulator provides an effective tool for EM prediction of multi-layer interconnects, covering the advanced material, flexible current operation, varying temperature and different interconnect architecture at scaled technology node.

ACKNOWLEDGMENT

This work is supported by National Natural Science Foundation of China 2016YFA0202101, No. 61674008, No. 61421005.

REFERENCES

[1] D. Prasad, and A. Naeemi, “Interconnect Design and Technology Optimization for Conventional and Emerging Nanoscale Devices: A Physical Design Perspective,” in IEEE International Electron Devices Meeting, pp. 103–106, Dec. 2018.

[2] International Technology Roadmap for Semiconductors, 2015, http://www.itrs2.net/itrs-reports.html.

[3] Szu-Tung Hu, Linjun Cao, Laura Spinella, and Paul S. Ho, “Microstructure Evolution and Effect on Resistivity for Cu Nanointerconnects and Beyond,” in IEEE International Electron Devices Meeting, pp. 115–117, Dec. 2018.

[4] S. V. Kolesnikov, A. M. Saletsky, S. A. Dokukin, and A. L. Klavsyuk, “Kinetic Monte Carlo Method: Mathematical Foundations and Applications for Physics of Low-Dimensional Nanostructures,” Mathematical Models and Computer Simulations, vol. 10, pp. 564-587, 2018.

[5] Cher Ming Tan, Zhenghao Gan, Wei Li, and Yuejin Hou, “Applications of Finite Element Methods for Reliability Studies on ULSI Interconnections,” *Springer*, pp. 73-110, 2011.

[6] J. R. Lloyd, J. Clemnes, and R. Snede, “Copper metallization reliability,” Microelectronics Reliability, vol. 39, pp. 1595–1602, Nov. 1999.

[7] Y. D. Zhao, P. Huang, Z. H. Guo, Z. Y. Lun, B. Gao, X. Y. Liu, and J. F. Kang, “Atomic Monte-Carlo Simulation for CBRAM with Various Filament Geometries,” in International Conference on Simulation of Semiconductor Processes and Devices, pp. 153-156, Sept. 2016.

[8] Shidong Li, Michael S. Sellers, Cemal Basaran, Andrew J. Schultz, and David A. Kofke, “Lattice Strain Due to an Atomic Vacancy,” International Journal of Molecular Sciences, vol. 10, pp. 2798-2808, June 2009.

[9] Yudi Zhao, Peng Huang, Zhe Chen, Chen Liu, Haitong Li, Bing Chen, Wenjia Ma, Feifei Zhang, Bin Gao, Xiaoyan Liu, and Jinfeng Kang, “Modeling and Optimization of Bilayered Ta*Ox* RRAM Based on Defect Evolution and Phase Transition Effects,” IEEE Trans. Electron Devices, vol. 63, pp. 1524-1532, April 2016.

[10] Hui Zheng, Binfeng Yin, Ke Zhou, Leigang Chen, and Chinte Kuo, “Temperature-dependent activation energy of electromigration in Cu/porous low-k interconnects,” Journal of Applied Physics, vol. 122, pp. 074501-1-7, August 2017.

[11] Seungman Choi, Cathryn Christiansen, Linjun Cao, James Zhang, Ronald Filippi, Tian Shen, Kong Boon Yeap, Sean Ogden, Haojun Zhang, Bianzhu Fu, and Patrick Justison, “Effect of Metal Line Width on Electromigration of BEOL Cu Interconnects”, in International Reliability Physics Symposium, pp. 4F.4-1-6, March 2018.

[12] A. S. Oates, and M. H. Lin, “Analysis and modeling of critical current density effects on electromigration failure distributions of Cu dual-damascene vias,” in International Reliability Physics Symposium, pp. 385-391, April 2008.